

pubs.acs.org/acssensors Article

A Low-Cost, Tabletop LOD-EPR System for Nondestructive Quantification of Iron Oxide Nanoparticles in Tissues

Saurin Kantesaria, Xueyan Tang, Steven Suddarth, Jacqueline Pasek-Allen, Bat-Erdene Namsrai, Arjun Goswitz, Mikaela Hintz, John Bischof, and Michael Garwood*



Cite This: https://doi.org/10.1021/acssensors.3c01898



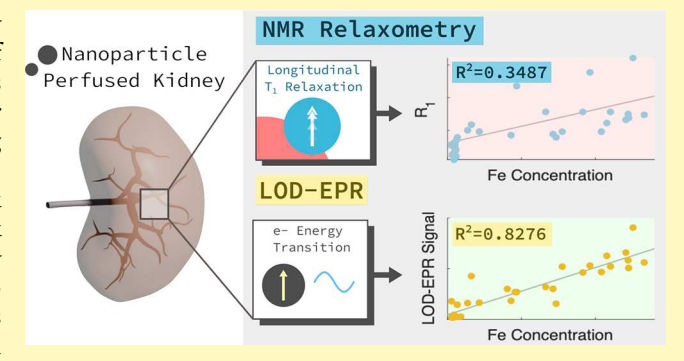
ACCESS I

III Metrics & More

Article Recommendations

supporting Information

ABSTRACT: Iron oxide nanoparticles (IONPs) have wide utility in applications from drug delivery to the rewarming of cryopreserved tissues. Due to the complex behavior of IONPs (e.g., uneven particle distribution and aggregation), further developments and clinical translation can be accelerated by having access to a noninvasive method for tissue IONP quantification. Currently, there is no low-cost method to nondestructively track IONPs in tissues across a wide range of concentrations. This work describes the performance of a low-cost, tabletop, longitudinally detected electron paramagnetic resonance (LOD-EPR) system to address this issue in the field of cryopreservation, which utilizes IONPs for rewarming of rat kidneys. A low-cost LOD-EPR system is realized via simultaneous transmit and receive using MHz



continuous-wave transverse excitation with kHz modulation, which is longitudinally detected at the modulation frequency to provide both geometric and frequency isolation. The accuracy of LOD-EPR for IONP quantification is compared with NMR relaxometry. Solution measurements show excellent linearity ($R^2 > 0.99$) versus Fe concentration for both measurements on EMG308 (a commercial nanoparticle), silica-coated EMG308, and PEG-coated EMG308 in water. The LOD-EPR signal intensity and NMR longitudinal relaxation rate constant (R_1) of water are affected by particle coating, solution viscosity, and particle aggregation. R_1 remains linear but with a reduced slope when in cryoprotective agent (CPA) solution, whereas the LOD-EPR signal is relatively insensitive to this. R_1 does not correlate well with Fe concentration in rat kidney sections ($R^2 = 0.3487$), while LOD-EPR does ($R^2 = 0.8276$), with a linear regression closely matching that observed in solution and CPA.

KEYWORDS: iron oxide nanoparticles, low frequency, electron paramagnetic resonance, nuclear magnetic resonance, cryopreservation

Iron oxide and other biocompatible magnetic nanostructures continue to be valuable materials for biomedical applications. Iron oxide nanoparticles (IONPs) vary in size and structure but are typically spherical structures composed of magnetite (Fe₃O₄). Most common applications in biomedical research include the delivery of drugs, hyperthermia-based treatment of tumors, point-of-care disease detection, and many others. Utilization of IONPs for nanowarming of tissues has emerged as another useful application of IONPs for rapid rewarming of cryopreserved tissues to physiologic temperatures prior to transplant.

About 20% of kidneys donated for transplant are discarded due to short storage viability (~24–36 h). 4,5 Cryopreservation decreases storage temperatures below –140 °C, enabling the storage of kidneys and other organs for months to years. To avoid damage to cells due to ice formation and physical organ cracking, fast and even warming is needed to reheat cryopreserved organs. For this, IONPs can be perfused into organs prior to cooling, and then, radiofrequency (RF) irradiation can be applied to rapidly rotate their magnetic

moments, causing local heating around IONPs and organ rewarming.^{6,7} This so-called nanowarming technology for cryopreservation has been successfully demonstrated on rat kidneys perfused with IONPs and cryoprotective agents (CPAs) that prevent ice formation.⁸

Nanowarming and other emerging applications of IONPs are in need of quantitative measuring tools that can help elucidate the complex behaviors of IONPs in tissues (distribution, protein/ion-induced particle aggregation, rotational restriction, etc.) that currently limit reproducibility and translation to human organs. There is a need for precise monitoring of IONP concentrations (1) after perfusing them into organs to ensure even IONP distribution and, therefore,

Received: September 10, 2023 Revised: November 15, 2023 Accepted: December 1, 2023



even kidney heating and viability and (2) prior to transplant, to prevent potential IONP-related iron toxicity post-transplant (Figure 1). At present, there is no low-cost method to nondestructively track IONPs across concentrations of interest (0.01–100 mg Fe/mL).

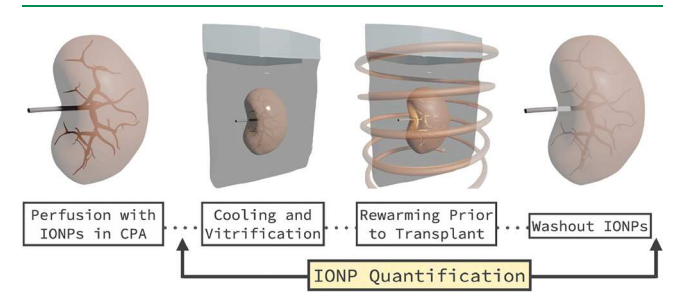


Figure 1. General workflow for kidney cryopreservation and nanowarming, with points for IONP quantification highlighted.

A general range of 0.01-100 mg Fe/mL is assumed for nanowarming based on the lower range of IONP concentrations that have safely remained in kidneys postwashout9 and the potential upper range of IONP concentrations that could be used with more recently developed IONP coatings for nanowarming. 10 While a specific accuracy tolerance for nanowarming has not yet been established, it is an area of active study, as the IONP Fe concentration is directly proportional to the warming rate. However, for reference, a tolerance for rewarming of 72 \pm 8 °C/min was achieved in the kidneys that were successfully vitrified, nanowarmed, and transplanted for 30 days, with an estimated rewarming threshold of 50 °C/min. Further study is needed to establish the precise threshold for failure and appropriate tolerances to mitigate the associated risks; however, the required accuracy for quantifying the IONP Fe concentration will be reflective of this analysis.

Current methods of quantifying IONPs in tissues (Table 1) include NMR/MRI^{11,12} (see Figure 2), micro-CT, magnetic particle imaging (MPI), magnetic particle spectroscopy (MPS), and inductively coupled plasma-mass spectroscopy (ICP-MS), seach of which has pros and cons. NMR and MRI enable the quantification of tissue IONPs by exploiting the interaction between unpaired Fe electrons and the H protons of the tissue water molecules. This interaction leads to a shortening of the longitudinal relaxation time constant (T_1) of the NMR/MRI signals, and based on the measured relationship between T_1 and Fe concentration, the tissue Fe concentration can be estimated. Unfortunately, the detection range of these MR methods is limited by the inability of

hardware to measure the extremely short T_1 values that exist for protons in H₂O in high iron concentration environments. Further, while NMR has excellent sensitivity, the sample volume is typically limited and would require organ biopsies for any form of spatial resolution. On the other hand, micro-CT cannot detect low concentrations of IONPs and has limited insight into particle behavior in tissues as it primarily detects IONPs by physical density differences with the surrounding tissue. Magnetic particle imaging has good sensitivity and specificity; however, it is costly even for rodent-scale systems (~\$1 million per scanner), and the power requirements for larger specimens are likely to require superconducting technology to achieve the required fields. 18-21 Alternatively, for bulk sample quantitation, the spectroscopic version of magnetic particle imaging, magnetic particle spectroscopy, provides excellent sensitivity.²² Finally, ICP-MS is the gold standard method for iron quantification with excellent sensitivity; however, it is destructive and costly and gives no information on spatial distribution/particle behavior. It is important to mention that imaging systems require more hardware and technical complexity than systems that provide bulk quantitative information on samples; thus, for direct comparisons, methods such as NMR, MPS, and ICP-MS are most comparable in contrast to systems such as MRI. MPI, and micro-CT. As such, NMR and MPI appear to be the most promising methods that currently exist, but both are costly and limited by the sample volume.

Our lab has developed a low-cost, longitudinally detected electron paramagnetic resonance (LOD-EPR) system that directly detects electrons from iron in IONPs (Figure 3). Preliminary data ^{23,24} suggest that LOD-EPR is sensitive to IONP concentration in solution. By having a transmit frequency in the MHz range, which has a higher penetration depth than other EPR systems which transmit in the GHz range, our system can be scaled to human organs as well. This system would serve as a low-cost tool to understand the IONP behavior in cryopreserved kidneys and other tissues. This would allow troubleshooting of IONP coatings to prevent aggregation, tuning of RF heating based on IONP distribution, and determination of points of IONP accumulation to overcome current failure points in kidney cryopreservation.

NMR and MRI are the most common of the above methods for quantifying IONPs and thus will be the method of choice to compare to our LOD-EPR system.

Our LOD-EPR system (Figure 3) senses at low magnetic fields (<300 G) and frequencies (MHz) at room temperature using a simultaneous transmit and receive (STAR) sensing method. The STAR method of acquisition here is primarily a result of the geometric isolation provided by our coil topology,

Table 1. Comparison of IONP Detection Methods

detection method	mechanism	approximate cost	approximate detection range [mg Fe/mL]	spatial resolution	sample size	destructive
benchtop NMR	IONP shortening H_2O T_1 relaxation	++	$>1 \times 10^{-511}$	-	+	yes
MRI	IONP shortening H_2O T_1 relaxation	+++	0-3 12	μ m $-$ mm	+++	no
micro-CT	IONP density	+++	>10 ²	μ m	+++	no
MPI	detection of IONP excitation harmonics	+++	$>6.7 \times 10^{-4}$ 13	mm	++	no
MPS	detection of IONP excitation harmonics	++	$>1 \times 10^{-3}$ 14	-	+++	no
ICP-MS	IONP chemical digestion + mass spectroscopy	++	$>1 \times 10^{-4} ^{15,16}$	-	+	yes
LOD-EPR	IONP e ⁻ moment	+	$> 8.65 \times 10^{-3} a$	mm	+++	no

^aExperimentally acquired result, see Figure 5.

NMR Relaxometry Longitudinal T₁ Relaxation | Felipse | Felipse

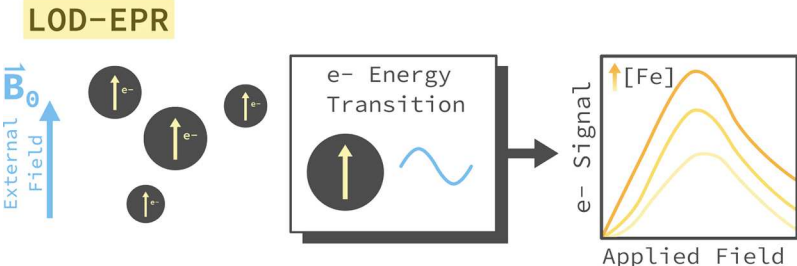


Figure 2. NMR relaxometry vs LOD-EPR general sensing mechanism. (top) Detection of IONPs (gray) with NMR relaxometry relies on detecting changes in the longitudinal relaxation time constant (T_1) of nearby water protons (^1H) . The local magnetic field of IONPs (dashed line) forms local field gradients that increase T_1 in a concentration-dependent manner. (bottom) Detection of IONPs with LOD-EPR relies on the direct detection of unpaired Fe electrons of IONPs. The external field (B_0) is increased across a sweep range until resonance is achieved in the form of a peak in the EPR spectrum. The height of this peak is dependent on the total number of unpaired electron spins.

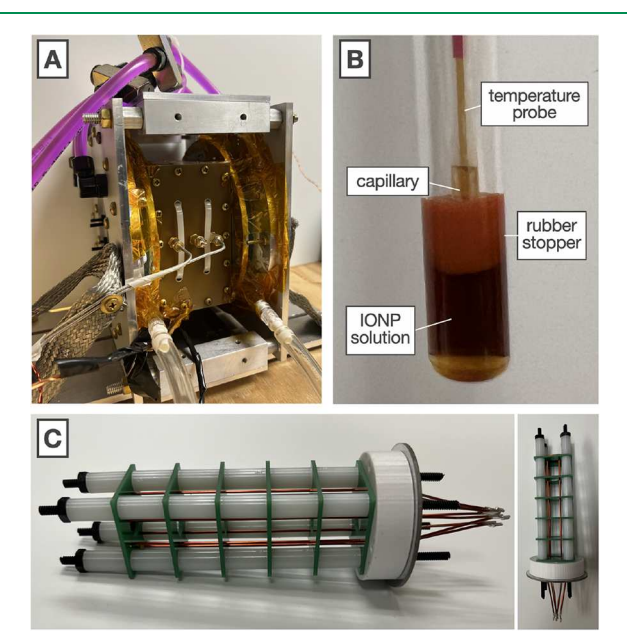


Figure 3. LOD-EPR system, sample setup, and transmit coil configuration. (A) The LOD-EPR system body is compact (roughly 0.5 ft \times 1 ft \times 1 ft) and able to fit on a lab bench. (B) The system is side-loaded; therefore, liquid samples need a rubber stopper. For direct solution temperature measurement, a glass capillary is embedded into the rubber stopper for ease of probe insertion into the solution. (C) The transmit coil is composed of two orthogonal long Helmholtz pairs driven independently in quadrature at an 11.53 MHz carrier frequency, with the amplitude modulated by a 47.8 kHz sinewave. The tuned/matched transmit coil is easily exchanged to allow for different carrier frequencies.

as the receive coil is perpendicular to the set of transmit coils. The frequency difference between the modulation (kHz) and carrier (MHz) also helps contribute to isolation. Finally, by exciting in the MHz range and sensing in the kHz range, penetration into aqueous samples is enabled using hardware

with less stringent sampling/output requirements than higher-frequency systems. These factors help contribute to a low-cost and compact system.

The LOD-EPR system employs a benchtop chiller, a rack-mounted power supply, and a pair of compact RF power amplifiers. We anticipate a significant reduction in size and cost by transitioning to a more efficient B_0 magnet and building customized hardware as opposed to relying on commercial general-purpose laboratory equipment.

Despite these advances, however, there is little literature on signal characteristics in these fields/frequencies. Here, we will compare the relationship of LOD-EPR and NMR signal to IONP concentration and behavior as well as the accuracy of overall IONP quantification in solution and in biopsies of rat kidneys perfused with IONPs.

MATERIALS AND METHODS

Materials. EMG308 was obtained from Ferrotec (nominal particle diameter of 10 nm). CPA components for the VMP in LM5 were purchased from Sigma-Aldrich. NMR tubes used were 7.5 mm in diameter.

EPR Instrumentation and Settings. The LOD-EPR system was custom-built as described previously; however, here, we briefly detail the setup.²³ There were two major fields generated for the experiment: one circularly polarized field along the xy-plane of the sample generated by the Hemholtz pair insert (Figure 3C) and another static B_0 field along the z-axis of the sample generated by the larger Hemholtz coils. To generate a spectrum, the transmit frequency was set to 11.53 MHz with an amplitude modulation of 47.8 kHz. This excitation field was applied to the xy-plane of the sample continuously, while the static B_0 field was applied along the z-axis of the sample. B_0 was stepped through the resonant peak of the sample and can be varied from -240 to 240 G. At the same time, the dM_z/dt of the bulk sample was collected by a z-oriented receive coil tuned to the modulation frequency at 47.8 kHz with a very high selectivity (Figure S1). A buffer size of 1×10^6 samples was collected from the receive coil signal, and the integrated signal energy was obtained over 25 averages. Since the LOD-EPR system is a side-loaded spectroscopy system, a rubber stopper was carefully pushed down each NMR tube to contain the solution to the bottom of the tube. A glass capillary (50

 μ L, 21-164-2G, Fisher Scientific) was embedded into the rubber stopper to allow for a temperature probe to measure the solution temperature during LOD-EPR measurements.

NMR Instrumentation and Settings. A Bruker Minispec mq60 benchtop NMR was used for the T_1 relaxometry of all solutions. Calibration was performed at the beginning of each day prior to measurements. The chiller temperature was set to 25 °C. A saturation recovery sequence was used for T_1 relaxometry (pulse length = 2.5 μ s, averages = 4). The minimum and maximum saturation delay times $T_{\rm SR}$ were set to ensure a full exponential curve with at least 3 points at the plateau. The gain was adjusted to ensure at least 90% of the full measurement range based on the fully relaxed case. Recycle delay was set to at least 5× the expected T_1 .

ICP-MS Instrumentation and Settings. ICP-MS was performed by ALS Global with an Agilent 7700. Solutions were sent as is in sealed containers for analysis by ICP-MS. Postperfusion and following measurement by NMR and LOD-EPR, tissues were dried in a vacuum oven overnight at 120 °C and powdered prior to shipping. The following procedure was provided by the company (ALS Global) performing ICP-MS: "A representative aliquot of the sample was added to a Teflon digestion vessel along with 15% concentrated nitric acid. If the sample was being analyzed by ICP, 15% concentrated nitric acid and 5% concentrated hydrochloric acid were used. The digestion vessel was then sealed and placed in a 105 °C oven for a minimum of 12 h. After cooling, the sample was transferred to a centrifuge tube and diluted to a 20 mL final volume with deionized water."

IONP Synthesis. EMG308 was obtained from Ferrotec and used in the synthesis of both silica- and PEG-coated IONPs. Synthesis procedures for sIONPs and pIONPs were performed as previously described.^{8,10} sIONPs had a coating thickness of approximately 18 nm.⁸ pIONPs did not have a measurable coating thickness as compared to bare EMG308.¹⁰

IONP and CPA Solution Preparation. The following solutions were made by using the above IONPs: EMG308 in Milli-Q water, sIONPs in Milli-Q water, pIONPs in Milli-Q water, and sIONPs in VMP in LM5. The IONPs in water solutions were diluted to estimated concentrations of 10, 5, 1, 0.5, and 0.05 mg Fe/mL. The lower limit of detection was determined for EMG308 by successive dilutions and measurements until the regression began to exhibit nonlinearity.

Each ordered batch of EMG308 was approximately 50 mg Fe/mL. The volume and mass changes during synthesis of sIONPs and pIONPs were recorded to give an estimated stock solution concentration. To further confirm the stock solution concentration, solutions were diluted to 0.5–2 mg Fe/mL in a glass ampule with 400 μ L of 100% nitric acid and Milli-Q water to a total volume of 600 μ L. The glass ampule was flame-sealed, and the solution was digested overnight at 80 °C. Three hundred μ L of the digestate was transferred to an NMR tube. R_1 (= $1/T_1$) was measured for each digestate and compared to a previously established calibration curve of digested Fe concentration verified by ICP-MS vs R_1 .

Three hundred μ L (3×) of each sample was prepared in NMR tubes for measurement of R_1 and LOD-EPR signal on each system. Solutions were sonicated for 2 min (4 s on, 2 s off, 20% power) and vortexed prior to measurement.

Solutions of sIONPs in the CPA were made by lyophilizing solutions of sIONPs in water. The lyophilized sIONPs were added to a CPA solution in a volumetric flask. To ensure complete disaggregation of sIONPs, they were bath sonicated for 1 h (37 kHz, 100% power, 25 °C, Elmasonic P) and probe sonicated in ice for 45 min (4 s on, 2 s off, 20% power, Qsonica) in 15 min intervals on the day before use. On the day of use, they were sonicated in ice for 45 min (4 s on, 2 s off, 20% power) in 15 min intervals and filtered through PET filters (pluriSelect pluriStrainer) at 40, 20, and 10 μ m and a glass fiber syringe filter (Tisch Scientific, 13 mm diameter) at 2.7 μ m.

Limit of Detection Calculation. The limit of detection was calculated for both NMR and LOD-EPR by performing a paired, two-tailed t-test between the 0 mg Fe/mL samples (n = 3) and

increasingly diluted concentrations (n=3) described in the IONP and CPA Solution Preparation section. Significance was shown for samples with $p \le 0.05$.

Aggregation Testing Sample Preparation. For the longer study, 2 sets of $3 \times 300~\mu\text{L}$ of 1 mg Fe/mL EMG308 in $1 \times$ PBS were prepared for measurement on NMR and LOD-EPR. Solutions were sonicated for 5 min (4 s on, 2 s off, 20% power) and vortexed prior to measurement on either NMR or LOD-EPR. The initial and aggregation states of the solutions were monitored using dynamic light scattering (DLS) by taking 2 μL aliquots of the solution. R_1 and LOD-EPR signal were measured repeatedly until steady-state aggregation was achieved. DLS was performed on the completely aggregated solutions.

For the shorter study, 2 sets of $3 \times 300~\mu\text{L}$ of 0.4 mg Fe/mL of each condition were prepared: EMG308 in $1\times$ and $5\times$ PBS and sIONPs in $1\times$ and $5\times$ PBS. Solutions were sonicated for 5 min (4 s on, 2 s off, 20% power) and vortexed prior to measurement. Each set was measured separately on NMR and LOD-EPR due to the speed of aggregation. Individual samples were measured at 0 min, 20 min, and 1 h.

Stability Testing Sample Preparation. Powdered DPPH (92.7 mg) was weighed in an NMR tube and measured repeatedly over the course of 1 month as an additional method to determine the repeatability of LOD-EPR on a stable paramagnetic solid. DPPH was stored at 4 °C and only exposed to light briefly during transfer from the refrigerator to the LOD-EPR (Figure S3).

Viscosity Testing Sample Preparation. Three hundred μL (3×) aliquots of ~1 mg Fe/mL EMG308 were prepared in mixtures of DMSO:H₂O (1:1), EG:H₂O (1:1, 1:4, and 3:4), and glycerol:H₂O (1:1). Solutions were sonicated for 2 min (4 s on, 2 s off, 20% power) and vortexed prior to measurement.

Tissue Sample Preparation. All animal experiments in this protocol (2204-39970A) were approved by the Institutional Animal Care and Use Committee (IACUC) at the University of Minnesota. Male Sprague-Dawley rats (10-12 weeks old, 300-400 g) were purchased from Charles River Laboratories (Wilmington, MA). Details of the surgery were performed as previously described.⁶ Rats underwent general anesthesia with isoflurane. The anesthesia depth was confirmed with a toe pinch reflex. The abdominal area was shaved and disinfected with a 70% ethanol solution. A transverse bilateral abdominal incision was performed, and the intestines were moved out of the abdomen. The abdominal aorta, inferior vena cava (IVC), left renal artery, and vein were mobilized for cannulation. 4.0-Silk loose ties were placed above the left renal artery, distal aorta, and IVC. Heparin (500 IU) was injected through the penile vein. Two minutes later, a loose tie was placed on the distal aorta, the IVC was tied, and a vascular bulldog clamp was placed distal to the renal artery to occlude the aorta for cannulation. The aorta was cannulated with a 20G bulb tip catheter (FTP-20-30, Instech Laboratories), and the vascular bulldog clamp was removed. The catheter was secured with a 4.0-silk tie and connected to a 10 mL syringe with cold (4 °C) University of Wisconsin (UW) solution mixed with 500 IU heparin. The loose tie above the left renal artery was tied, the infrahepatic IVC was vented, and the left kidney was perfused with cold UW solution. Once flushed, the cannulated left kidney was explanted and stored in a cold UW solution prior to perfusion.

Tissue Perfusion. Dissected rat kidneys were placed on a custom-built perfusion circuit connected to a chiller once the flow rate was calibrated, the system was flushed with water and 70% ethanol, and the chiller liquid was equilibrated to −7 °C. The kidney was kept in UW solution on ice, and connection to the renal artery was performed in solution to prevent air bubbles from entering the kidney. The kidney was ramp-loaded using the CPA-loading protocol described previously using VMP as the CPA and LMS as the carrier solution. For the conditions needing IONP perfusion, subsequently, the kidney was disconnected from the perfusion system and connected to a syringe pump set to 0.5 mL/min (diameter of 14.5 cm) loaded with 2.5 mL of sIONPs in VMP in LMS (either ∼5 or ∼10 mg Fe/mL). Kidneys with undesirably high pressure profiles (>60 mmHg) and/or

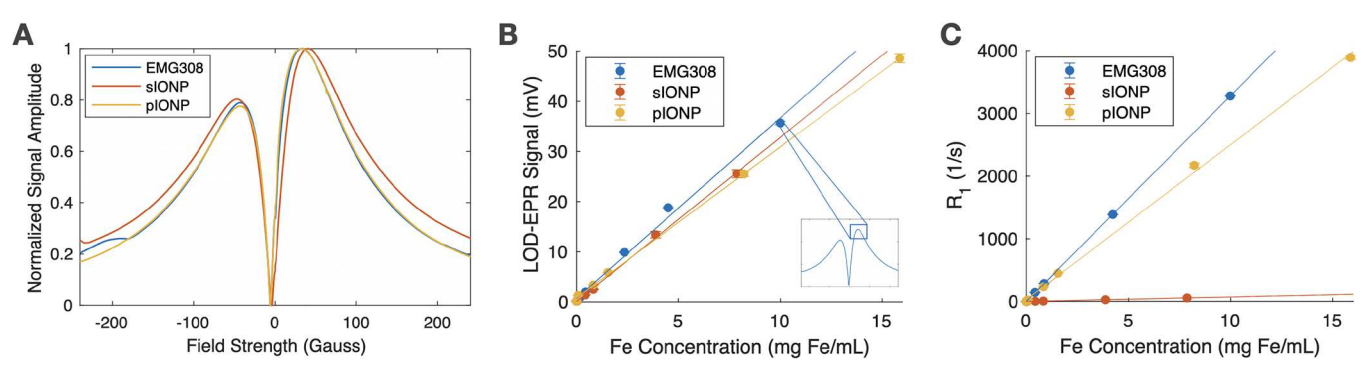


Figure 4. LOD-EPR full spectra and linear regressions vs R_1 . (A) Full LOD-EPR spectra of EMG308, sIONP, and pIONP samples at ~4 mg Fe/mL normalized to the maximum peak intensity. (B) Linear regressions of a 10-point average of the positive peak (inset) of the LOD-EPR spectrum vs Fe concentration for EMG308, sIONPs, and pIONPs in water. (C) Linear regressions of R_1 vs Fe concentration for EMG308, sIONPs, and pIONPs in water.

visually nonuniform perfusion were used for the poor perfusion conditions.

Analysis Methods. T_1 was obtained by built-in exponential fitting software in the NMR relaxometer. LOD-EPR signal was determined by sweeping over a range of B_0 values (typically between 0 and 80 G) until a peak was observed. A MATLAB script was written to extract a 10-point average around each peak for all spectra obtained.

■ RESULTS AND DISCUSSION

Effects of IONP Concentration and Coating. EMG308 is a cost-effective, commercially available nanoparticle that can be used for nanowarming; however, it is not very stable in CPA solutions. Thus, silica and PEG coatings have been applied to these particles. These may affect the slope and linearity of R_1 (= $1/T_1$) or LOD-EPR signal versus Fe concentration regressions; thus, these curves were investigated for each of these particles.

Linear regressions of Fe concentration (verified by ICP-MS) versus LOD-EPR signal (mV) and versus R_1 (s⁻¹) are shown for a single IONP with 3 types of coatings (EMG308, silicacoated IONPs, and PEG-coated IONPs) (Figure 4). Linear regressions for all particles on both NMR and LOD-EPR demonstrate good fits but a change in the slope depending on the coating (Figure 4B,C). Relaxivity is reduced with the addition of a PEG coating and reduced further by the silica coating. By comparison, the LOD-EPR signal versus Fe concentration slopes are relatively close to each other (Figure 4B). The slope for EMG308 is higher than that of either the pIONPs or sIONPs, and the sIONPs only have a slightly higher slope than the pIONPs.

In the case of R_1 , the change in the slope is most likely a result of the variable separation of water molecules from the IONP core based on coating thickness. This would result in a lower local magnetic field affecting each water molecule and therefore a lower R_1 that can be seen for the slope of EMG308 as compared to the sIONP and pIONP slopes. The higher slope for the pIONPs compared to the sIONPs is expected as the PEG coating is thinner than the silica coating. Although further investigation is needed, one potential explanation for the observed change in LOD-EPR signal is that the surface spins on the IONPs change with different coatings.²⁵

Full LOD-EPR spectra normalized to the maximum peak intensity are shown (Figure 4A) for each of these particles from -240 to 240 G at approximately 4 mg Fe/mL. The shapes of the normalized spectra for EMG308 and pIONPs are roughly identical minus the beginnings of a wide-bandwidth

peak to the left of the EMG308 curve. The sIONP curve is slightly broader than either of these, with a small shift of the positive peak to the right. This may be related to coating synthesis, as pIONPs and EMG308 have similar coating thicknesses and primarily have one core per particle, whereas sIONPs have a large shell that sometimes encases more than one core per particle.

This same procedure was repeated for EMG308 in water at increasingly lower concentrations to compare the lower limit of detection for each system for this particular IONP in water (Figure 5). It was found that NMR had a lower limit of detection $(5.1 \times 10^{-5} \text{ mg Fe/mL})$ than the existing LOD-EPR system $(8.65 \times 10^{-3} \text{ mg Fe/mL})$.

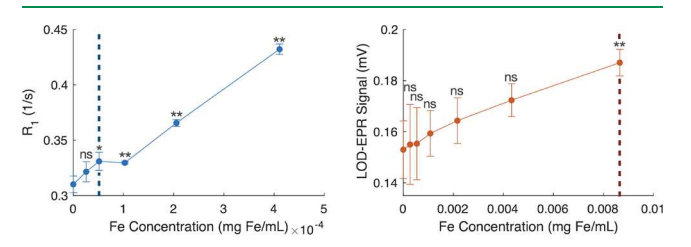


Figure 5. NMR has a lower limit of detection than LOD-EPR. Lower limit of detection comparison for EMG308 in water for (left) R_1 and (right) LOD-EPR. The lower limit of detection for NMR is approximately 5.1×10^{-5} mg Fe/mL. The lower limit of detection for LOD-EPR is approximately 8.65×10^{-3} mg Fe/mL. Asterisks and text indicate p-values from two-tailed paired t-tests when compared to 0 mg Fe/mL (ns = p > 0.05, *= p < 0.05).

EPR generally has better sensitivities than NMR due to the increased electron gyromagnetic ratio among other factors; however, it is clear that the current LOD-EPR system requires further hardware refinements to match the sensitivity of a fully optimized commercial NMR system. There is still baseline noise variance that is above the thermal noise limit and that will need to be eliminated in future iterations of the system. The variance seen here is most likely a result of receive-related noise. Our receive coil is connected to the preamplifier via a coaxial cable wound around several low-frequency ferrites, but this does not completely eliminate external kHz noise sources. This issue would ideally be solved by the addition of an onboard preamplifier in the next iteration of our system. Other potential sources of noise include trace impurities within aluminum parts of the system or copper wires, as indicated by the small-amplitude (\sim 0.1 mV), broad-line-width background

spectrum that is observed when the system is run without any sample inserted. This will also be addressed in the next iteration of the system by minimizing usage of metal parts close to the transmit/receive coils and using 101 copper or silver wires.

Effects of Solution Viscosity on LOD-EPR Signal and R_1 . Solution viscosity may affect the rotational freedom of the easy axis of IONPs, which, in turn, would affect the alignment of both the internal magnetization of the particle and the alignment of water in close vicinity to the particle with the external field.

Two methods are used to determine the effects of viscosity on R_1 or LOD-EPR signal (Figure 6). Increasing the volume

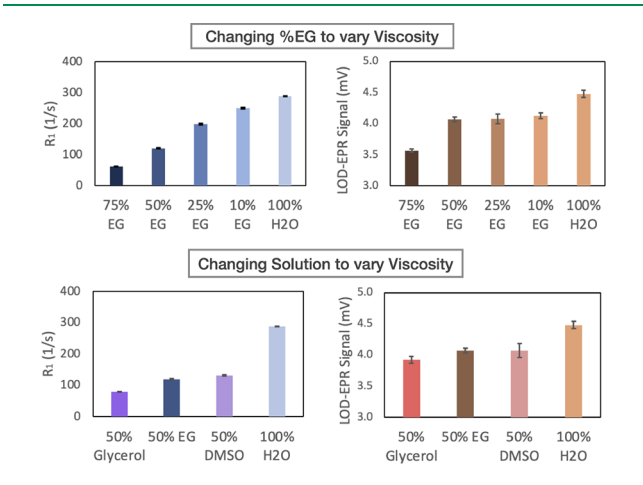


Figure 6. LOD-EPR signal and R_1 affected by solution viscosity. Comparison of LOD-EPR signal and R_1 in solutions of EMG308 by varying %EG by volume (top) and in solutions of increasing viscosity (glycerol > EG > DMSO > H_2O) (bottom) at 50% by volume.

percentage of ethylene glycol (EG) in solutions of 0.86 mg Fe/mL EMG308 decreases both R_1 and LOD-EPR signal. CPA components (glycerol and DMSO) with varying viscosity were also tested in a 1:1 ratio with deionized water.

Similar decreases in R_1 were seen for these solutions with increasing viscosity. The T_1 values of the hydrogen protons in glycerol, EG, and DMSO tend to be shorter than those of water. Furthermore, another study²⁶ has demonstrated that R_1 increases (shortening of T_1) with solution viscosity. Thus, the observed decrease in R_1 (increase in T_1) may result from the effect that viscosity has on particle rotation.

LOD-EPR signal decreases with solution viscosity, as shown for both scenarios. This again may be related to the effect of particle rotation on LOD-EPR signal as the easy axis of a given nanoparticle can be modeled as a separate magnetic field acting on the magnetization of an electron.^{27,28} If the rotation of this field is restricted, a decrease in the signal may be observed.

Effects of Aggregation on LOD-EPR Signal and R₁. Aggregation is an obvious concern when IONPs are introduced into the CPA and tissue, as the high concentration of sugars, salts, and proteins can cause aggregation due to electrostatic interactions and protein—protein bridging. This may affect the alignment of electron magnetization via coupling of electron moments and restricting the overall particle motion. Aggregation of multiple particles may also decrease the IONP surface area that is available to interact with the magnetic moment of the water protons.

Aggregation notably decreases both the LOD-EPR signal and R_1 over the course of slow complete sample aggregation for EMG308 in 1× PBS over the course of 4.5 months (Figure 7A). LOD-EPR signal decreases by approximately 62.3%, whereas R_1 decreases by approximately 99.8%.

While LOD-EPR decreases in signal for aggregated EMG308, this is not the case for aggregated sIONPs (Figure 7B). sIONPs in $5\times$ PBS aggregated completely over the course of 1 h. R_1 decreased by 84.0% over the hour, while LOD-EPR only experienced a slight initial decrease in signal of 4.1% and remained stable (<0.5% decrease) thereafter. sIONPs in $1\times$ PBS remained stable, and this is reflected in both the R_1 and LOD-EPR measurements remaining within 5% of their respective well-dispersed signal values.

Performing a similar test on EMG308 in 1× and 5× PBS over 1 h yielded more predictable results. EMG308 in 5× PBS

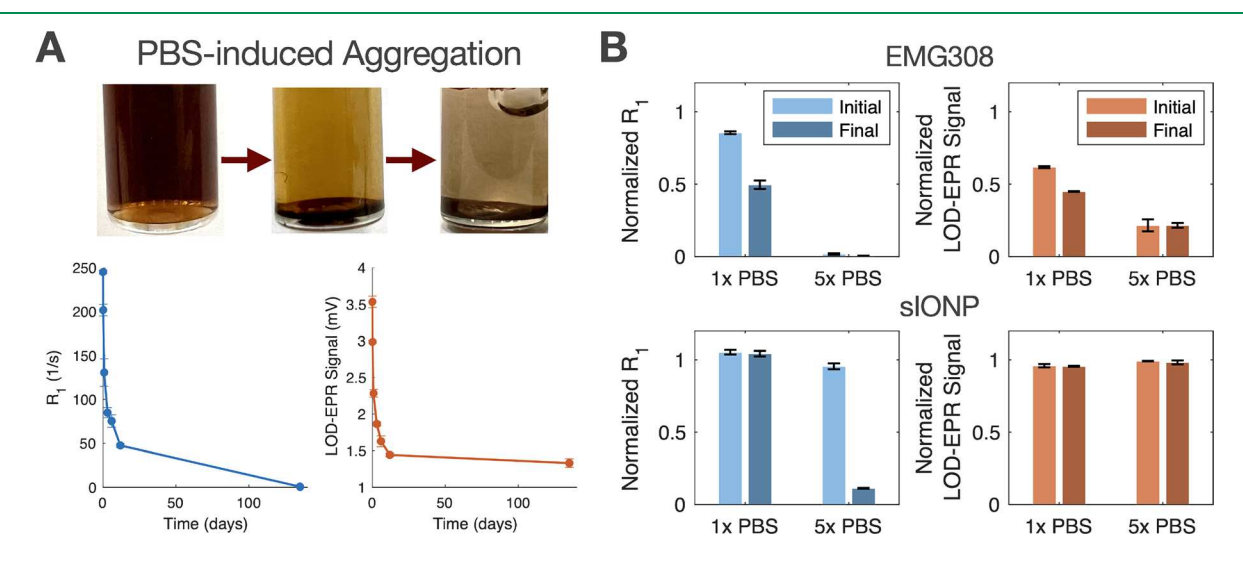


Figure 7. Aggregation decreases both R_1 and LOD-EPR signal. (A) Solutions of 1 mg Fe/mL EMG308 in 1× PBS throughout aggregation over the course of 4.5 months. Both R_1 (left) and LOD-EPR signal intensity (right) were measured until an apparent steady state was reached (n = 3 for each). (B) Similar aggregation study performed on 0.4 mg Fe/mL EMG308 (top) and sIONPs (bottom) over 1 h in both 1× PBS and 5× PBS. R_1 and LOD-EPR signals are normalized to signal values for a well-dispersed solution of each particle in water (n = 3 for each).

aggregated immediately on mixing. For this condition, R_1 decreased by 98.2%, and LOD-EPR signal decreased by 78.4% initially, with both decreasing minimally (<0.1%) after 1 h. EMG308 in 1× PBS aggregated slightly initially on mixing and continued to aggregate throughout the hour. For this condition, R_1 decreased initially by 14.5% and further by 35.9% (50.4% total signal decrease from well-dispersed), whereas LOD-EPR decreased initially by 38.2% and decreased further by 16.8% (55.1% total signal decrease from well-dispersed).

The decrease in the LOD-EPR signal can most likely be explained by several mechanisms. The field produced by one nanoparticle may affect the resonance frequency of adjacent particles as they come closer together with aggregation. This is most likely exaggerated for particles such as EMG308 with minimal coating thickness compared to sIONPs with considerable coating. A second mechanism may be that the easy axes of the IONPs in solution do not completely align with the external field, also causing a change in the resonance frequency. The former mechanism is further supported by the stability of the LOD-EPR signal for sIONPs even under extreme aggregation conditions, suggesting that the shell prevents this interaction from occurring.

The decrease in R_1 is most likely a result of aggregation and subsequent sedimentation of the particles within the NMR tubes, potentially accelerated by the field of the NMR relaxometer. As more particles aggregate, the surface area of particles exposed to water decreases. This is further exacerbated by the particles crashing out of solution to the bottom of the tube such that only the bottom layer of water molecules is exposed to the bulk of the particles. Therefore, on complete aggregation, the R_1 value will be close to that of water on this NMR system (\sim 0.3 s⁻¹).

Notably, there was a mismatch (\sim 30%) between the predicted R_1 and LOD-EPR signals for the concentration of particles used for the sIONPs used in the aggregation study. This may be a result of oxidation of the particles, ²⁹ geometrical frustration of the spins within the particles, ³⁰ or other phenomena. To allow for a comparison of the data between experiments, the data have been normalized to a well-dispersed solution of each particle.

Effects of the CPA on LOD-EPR Signal and R_1 **.** The net effect of switching the surrounding solution from water to a CPA (e.g., viscosity-related effects, inherent changes in R_1 , etc.) is of interest as cryobiologists utilize many different CPA formulations, which continue to evolve. Knowing the effects of the CPA on the slope of R_1 and the LOD-EPR signal versus Fe concentration would help inform whether a new calibration curve is needed for every CPA or simply for each particle.

Switching the surrounding solution with a CPA such as VMP/LM5 notably reduces the relaxivity of water, as shown (Figure 8). In contrast, this has a minimal effect on the slope of LOD-EPR signal versus Fe concentration (\sim 20% difference between values on each line). While linearity is excellent for both scenarios, this demonstrates that one would need a separate linear regression of R_1 versus Fe concentration for each CPA using NMR, whereas LOD-EPR, being relatively insensitive to these effects, could potentially need only one depending on the level of accuracy needed and the concentration range.

LOD-EPR Signal and R_1 in CPA- and IONP-Perfused Rat Kidney Sections. Lastly but most importantly, determining the accuracy of mapping the net tissue R_1 and LOD-EPR signal to an Fe concentration in rat kidneys will

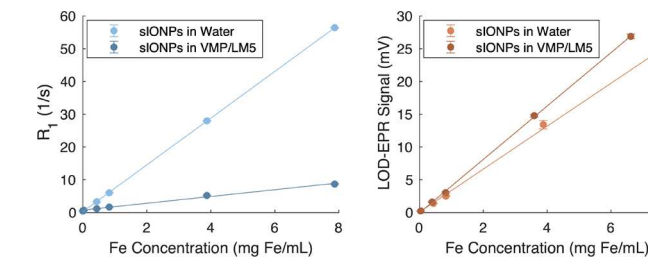


Figure 8. LOD-EPR minimally affected by changing the IONP surrounding solution from water to CPA. Solutions of sIONPs in Milli-Q water and sIONPs in VMP in LM5 at varying Fe concentrations (n=3 per point). Different linear regressions of R_1 vs Fe concentration (left) are seen for sIONPs in water (y=1.04x+0.76, $R^2=1.000$) and sIONPs in VMP in LM5 (y=7.13x+0.29, $R^2=9949$). Similar linear regressions of LOD-EPR signal vs Fe concentration (right) are seen for sIONPs in water (y=3.27x+0.08, $R^2=9994$) and sIONPs in VMP in LM5 (y=4.07x-0.03, $R^2=0.9998$).

help determine the utility of using R_1 or LOD-EPR for quantifying IONP concentrations in tissues when all of the above factors and others are accounted for.

 R_1 and a mass-corrected LOD-EPR signal versus Fe concentration from sections (n=5-6) of rat kidneys perfused with varying concentrations of sIONPS in VMP in LM5 are shown (Figure 9). To examine the performance of each system for nonideal perfusions related to particle aggregation, uneven perfusion, and similar issues, two additional kidneys with intentionally poor perfusion were included at 5 and 10 mg Fe/mL loading solution concentrations. A perfusion is designated as poor when there is an initial inlet pressure increase well above standard pressures. This suggests that an occlusion was introduced during the perfusion, typically an air bubble blocking the vasculature or incomplete filtration of perfusion solutions.

 R_1 shows poor linearity when compared with Fe concentration. LOD-EPR signal is divided by the mass of the tissue section since, unlike the solution measurements, the sample sizes are not the same. Notably, the mass-corrected LOD-EPR signal demonstrates good linearity over the Fe concentrations tested.

The lack of overall linearity in R_1 vs Fe concentration measurements can be explained by the heterogeneity of interand intrakidney R_1 . Notably, the fresh and CPA-loaded conditions demonstrate widespread R_1 values. LOD-EPR is insensitive to these effects since the primary signal is from electrons in Fe within the nanoparticle. The observed linearity between the LOD-EPR signal and Fe concentration in the kidney tissues is not as good as that observed in the solutions but may be adequate for quantification in many experimental applications, including nanowarming. Errors seen in this study may be a combination of aggregation effects, inherent tissue Fe (ICP-MS cannot differentiate between tissue Fe and nanoparticle Fe), incomplete digestion of tissue samples, and errors in quantifying the tissue mass.

CONCLUSIONS

Here, we show the performance of a custom-built, tabletop LOD-EPR system in quantifying IONPs in tissues when compared with a commercial tabletop NMR system functioning as a T_1 relaxometer. It is shown that the IONP coating, solution viscosity, and IONP aggregation affect both LOD-

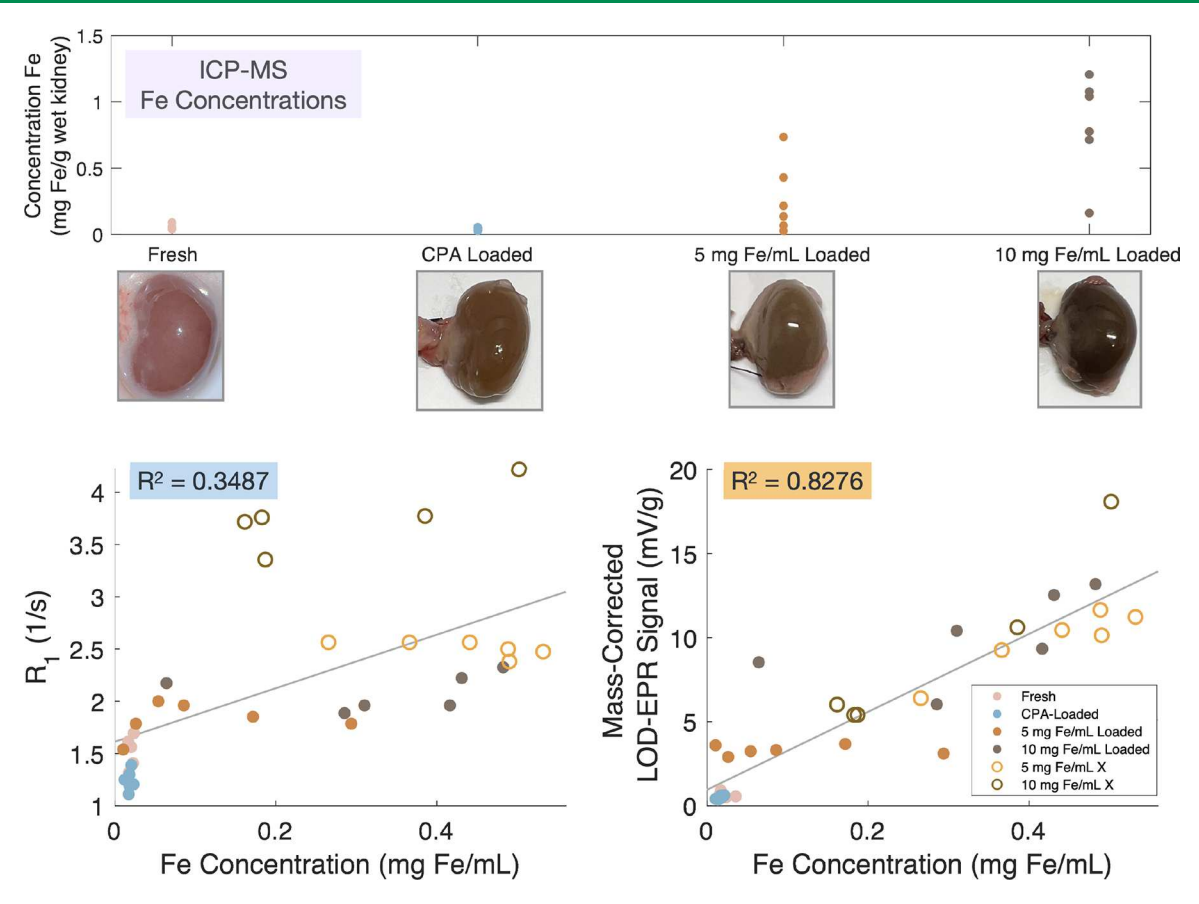


Figure 9. LOD-EPR demonstrates stronger correlation to Fe concentration in tissues than R_1 . Rat kidneys were sectioned into n = 5-6 sections and measured on both systems either directly after dissection and flushing (fresh), after loading with CPA, or after loading with 5 and 10 mg Fe/mL solutions of sIONPs in the CPA for kidneys with uniform and poor (X) perfusion. (left) R_1 and (right) LOD-EPR signal corrected by the mass of the kidney section vs ICP-verified Fe concentration is shown for each section of a given condition. Correlation for R_1 vs Fe concentration ($R^2 = 0.3487$) is significantly lower than that of mass-corrected LOD-EPR signal vs Fe concentration ($R^2 = 0.8276$).

EPR signal and NMR signal relaxation. Unlike R_1 , LOD-EPR is insensitive to a change in the surrounding solution (including the tissue), making it more practical for establishing a calibration curve for Fe concentration versus signal for a given particle. The current iteration of the LOD-EPR system has a higher limit of detection than the benchtop NMR system; however, further hardware improvements (an onboard preamplifier, further transmit filtering, etc.) are expected to improve the signal-to-noise ratio to ideally match or surpass this. Lastly and most importantly, R₁ varies widely between kidneys and within a given kidney, making IONP quantification difficult, whereas LOD-EPR maintains linearity of Fe concentration versus signal intensity under these conditions. Overall, LOD-EPR has great potential as an affordable tabletop method of quantifying IONPs in tissues. Future work will include hardware improvements to this system, increasing the size of the bore for accommodation of whole kidneys and eventually designing the system for EPR imaging of the distributions of IONPs in tissues.

ASSOCIATED CONTENT

Supporting Information

The Supporting Information is available free of charge at https://pubs.acs.org/doi/10.1021/acssensors.3c01898.

Receiving system selectivity vs probe coil frequency (Figure S1), LOD-EPR signal vs sample temperature (Figure S2), LOD-EPR signal reproducibility (Figure

S3), and iron concentration in IONP-perfused rat kidneys validated by ICP-MS (Figure S4) (PDF)

AUTHOR INFORMATION

Corresponding Author

Michael Garwood — Center for Magnetic Resonance Research and Department of Radiology, University of Minnesota, Minneapolis, Minnesota 55455, United States; Email: gar@ umn.edu

Authors

Saurin Kantesaria — Center for Magnetic Resonance Research and Department of Radiology, University of Minnesota, Minneapolis, Minnesota 55455, United States; Department of Biomedical Engineering, University of Minnesota, Minneapolis, Minnesota 55455, United States; orcid.org/0000-0001-5495-836X

Xueyan Tang – Center for Magnetic Resonance Research and Department of Radiology, University of Minnesota, Minneapolis, Minnesota 55455, United States

Steven Suddarth – Center for Magnetic Resonance Research and Department of Radiology, University of Minnesota, Minneapolis, Minnesota 55455, United States

Jacqueline Pasek-Allen – Department of Biomedical Engineering, University of Minnesota, Minneapolis, Minnesota 55455, United States

- Bat-Erdene Namsrai Department of Surgery, University of Minnesota, Minneapolis, Minnesota 55455, United States
- Arjun Goswitz Department of Mechanical Engineering, University of Minnesota, Minneapolis, Minnesota 55455, United States
- Mikaela Hintz Department of Mechanical Engineering, University of Minnesota, Minneapolis, Minnesota 55455, United States
- John Bischof Department of Biomedical Engineering, University of Minnesota, Minneapolis, Minnesota 55455, United States; Department of Mechanical Engineering, University of Minnesota, Minneapolis, Minnesota 55455, United States; oorcid.org/0000-0001-6726-7111

Complete contact information is available at: https://pubs.acs.org/10.1021/acssensors.3c01898

Notes

The authors declare no competing financial interest.

ACKNOWLEDGMENTS

This material is based upon work supported by the National Science Foundation under Grant No. EEC 1941543 and The Malcolm B. Hanson Endowed Chair in Radiology. We also thank Dr. Zonghu Han for his guidance in kidney perfusion and Michael Etheridge for his advice during the revision process.

ABBREVIATIONS

LOD-EPR, longitudinally detected electron paramagnetic resonance; IONP, iron oxide nanoparticle; sIONP, silicacoated iron oxide nanoparticle; pIONP, polyethylene glycolcoated iron oxide nanoparticle; CPA, cryoprotective agent; MPI, magnetic particle imaging; MPS, magnetic particle spectroscopy; ICP-MS, inductively coupled plasma-mass spectroscopy

■ REFERENCES

- (1) Estelrich, J.; Escribano, E.; Queralt, J.; Busquets, M. A. Iron Oxide Nanoparticles for Magnetically-Guided and Magnetically-Responsive Drug Delivery. *International Journal of Molecular Sciences* **2015**, *16* (4), 8070–8101.
- (2) Gneveckow, U.; Jordan, A.; Scholz, R.; Brüß, V.; Waldöfner, N.; Ricke, J.; Feussner, A.; Hildebrandt, B.; Rau, B.; Wust, P. Description and Characterization of the Novel Hyperthermia- and Thermoablation-System for Clinical Magnetic Fluid Hyperthermia. *Medical Physics* **2004**, *31* (6), 1444–1451.
- (3) Yuen, C.; Liu, Q. Magnetic Field Enriched Surface Enhanced Resonance Raman Spectroscopy for Early Malaria Diagnosis. *J. Biomed Opt* **2012**, *17* (1), No. 017005.
- (4) Lewis, J. K.; Bischof, J. C.; Braslavsky, I.; Brockbank, K. G. M.; Fahy, G. M.; Fuller, B. J.; Rabin, Y.; Tocchio, A.; Woods, E. J.; Wowk, B. G.; Acker, J. P.; Giwa, S. The Grand Challenges of Organ Banking: Proceedings from the First Global Summit on Complex Tissue Cryopreservation. *Cryobiology* **2016**, *72* (2), 169–182.
- (5) Organ Donation and Transplantation Statistics. National Kidney Foundation. https://www.kidney.org/news/newsroom/factsheets/Organ-Donation-and-Transplantation-Stats 2016.
- (6) Sharma, A.; Rao, J. S.; Han, Z.; Gangwar, L.; Namsrai, B.; Gao, Z.; Ring, H. L.; Magnuson, E.; Etheridge, M.; Wowk, B.; Fahy, G. M.; Garwood, M.; Finger, E. B.; Bischof, J. C. Vitrification and Nanowarming of Kidneys. *Adv. Sci.* (Weinh) **2021**, 8 (19), No. e2101691.
- (7) Etheridge, M. L.; Bischof, J. C. Optimizing Magnetic Nanoparticle Based Thermal Therapies Within the Physical Limits of Heating. *Ann. Biomed Eng.* **2013**, *41* (1), 78–88.

- (8) Gao, Z.; Ring, H. L.; Sharma, A.; Namsrai, B.; Tran, N.; Finger, E. B.; Garwood, M.; Haynes, C. L.; Bischof, J. C. Preparation of Scalable Silica-Coated Iron Oxide Nanoparticles for Nanowarming. *Advanced Science* **2020**, *7* (4), 1901624.
- (9) Han, Z.; Rao, J. S.; Gangwar, L.; Namsrai, B.-E.; Pasek-Allen, J. L.; Etheridge, M. L.; Wolf, S. M.; Pruett, T. L.; Bischof, J. C.; Finger, E. B. Vitrification and Nanowarming Enable Long-Term Organ Cryopreservation and Life-Sustaining Kidney Transplantation in a Rat Model. *Nat. Commun.* **2023**, *14* (1), 3407.
- (10) Pasek-Allen, J. L.; Wilharm, R. K.; Gao, Z.; Pierre, V. C.; Bischof, J. C. Phosphonate Coating of Commercial Iron Oxide Nanoparticles for Nanowarming Cryopreserved Samples. *J. Mater. Chem. B* **2022**, *10* (19), 3734–3746.
- (11) Gunn, J.; Paranji, R. K.; Zhang, M. A Simple and Highly Sensitive Method for Magnetic Nanoparticle Quantitation Using 1H-NMR Spectroscopy. *Biophys. J.* **2009**, 97 (9), 2640–2647.
- (12) Etheridge, M. L.; Hurley, K. R.; Zhang, J.; Jeon, S.; Ring, H. L.; Hogan, C.; Haynes, C. L.; Garwood, M.; Bischof, J. C. Accounting for Biological Aggregation in Heating and Imaging of Magnetic Nanoparticles. *Technology* **2014**, *2*, 214–228.
- (13) Paysen, H.; Loewa, N.; Weber, K.; Kosch, O.; Wells, J.; Schaeffter, T.; Wiekhorst, F. Imaging and Quantification of Magnetic Nanoparticles: Comparison of Magnetic Resonance Imaging and Magnetic Particle Imaging. *J. Magn. Magn. Mater.* **2019**, 475, 382–388.
- (14) Paysen, H.; Wells, J.; Kosch, O.; Steinhoff, U.; Trahms, L.; Schaeffter, T.; Wiekhorst, F. Towards Quantitative Magnetic Particle Imaging: A Comparison with Magnetic Particle Spectroscopy. *AIP Advances* **2018**, *8* (5), No. 056712.
- (15) Chertok, B.; Cole, A. J.; David, A. E.; Yang, V. C. Comparison of Electron Spin Resonance Spectroscopy and Inductively-Coupled Plasma Optical Emission Spectroscopy for Biodistribution Analysis of Iron-Oxide Nanoparticles. *Mol. Pharmaceutics* **2010**, 7 (2), 375–385.
- (16) Gobbo, O. L.; Wetterling, F.; Vaes, P.; Teughels, S.; Markos, F.; Edge, D.; Shortt, C. M.; Crosbie-Staunton, K.; Radomski, M. W.; Volkov, Y.; Prina-Mello, A. Biodistribution and Pharmacokinetic Studies of SPION Using Particle Electron Paramagnetic Resonance, MRI and ICP-MS. *Nanomedicine* **2015**, *10* (11), 1751–1760.
- (17) Jeon, M.; Halbert, M. V.; Stephen, Z. R.; Zhang, M. Iron Oxide Nanoparticles as T1 Contrast Agents for Magnetic Resonance Imaging: Fundamentals, Challenges, Applications, and Prospectives. *Adv. Mater.* **2021**, 33 (23), 1906539.
- (18) Le, T.-A.; Bui, M. P.; Gadelmowla, K. M.; Oh, S.; Yoon, J. First Human-Scale Magnetic Particle Imaging System with Superconductor. *Int. J. Magn. Part. Imaging IJMPI* **2023**, 9 (1 Suppl 1). DOI: 10.18416/IJMPI.2023.2303032.
- (19) Gleich, B.; Weizenecker, J. Tomographic Imaging Using the Nonlinear Response of Magnetic Particles. *Nature* **2005**, 435 (7046), 1214–1217.
- (20) Weizenecker, J.; Borgert, J.; Gleich, B. A Simulation Study on the Resolution and Sensitivity of Magnetic Particle Imaging. *Phys. Med. Biol.* **2007**, *52* (21), 6363–6374.
- (21) Panagiotopoulos, N. Magnetic Particle Imaging: Current Developments and Future Directions. *Int. J. Nanomedicine* **2015**, *10*, 3097–3114.
- (22) Löwa, N.; Seidel, M.; Radon, P.; Wiekhorst, F. Magnetic Nanoparticles in Different Biological Environments Analyzed by Magnetic Particle Spectroscopy. *J. Magn. Magn. Mater.* **2017**, 427, 133–138.
- (23) Tang, X.; Suddarth, S.; Qian, G.; Garwood, M. Ultra-Low Frequency EPR Using Longitudinal Detection and Fictitious-Field Modulation. *J. Magn. Reson.* **2020**, *321*, No. 106855.
- (24) Tang, X.; Suddarth, S.; Kantesaria, S.; Garwood, M. A Frequency-Swept, Longitudinal Detection EPR System for Measuring Short Electron Spin Relaxation Times at Ultra-Low Fields. *J. Magn. Reson.* **2022**, 342, No. 107279.
- (25) Lak, A.; Disch, S.; Bender, P. Embracing Defects and Disorder in Magnetic Nanoparticles. *Advanced Science* **2021**, *8* (7), 2002682.

- (26) Bloembergen, N.; Purcell, E. M.; Pound, R. V. Relaxation Effects in Nuclear Magnetic Resonance Absorption. *Phys. Rev.* **1948**, 73 (7), 679–712.
- (27) Ota, S.; Ohkawara, S.; Hirano, H.; Futagawa, M.; Takemura, Y. Empirical and Simulated Evaluations of Easy-Axis Dynamics of Magnetic Nanoparticles Based on Their Magnetization Response in Alternating Magnetic Field. *J. Magn. Magn. Mater.* **2021**, 539, No. 168354.
- (28) Shah, S. A.; Reeves, D. B.; Ferguson, R. M.; Weaver, J. B.; Krishnan, K. M. Mixed Brownian Alignment and Néel Rotations in Superparamagnetic Iron Oxide Nanoparticle Suspensions Driven by an Ac Field. *Phys. Rev. B* **2015**, 92 (9), No. 094438.
- (29) Tang, J.; Myers, M.; Bosnick, K. A.; Brus, L. E. Magnetite Fe3O4 Nanocrystals: Spectroscopic Observation of Aqueous Oxidation Kinetics. *J. Phys. Chem. B* **2003**, *107* (30), 7501–7506.
- (30) Shendruk, T. N.; Desautels, R. D.; Southern, B. W.; van Lierop, J. The Effect of Surface Spin Disorder on the Magnetism of γ -Fe2O3 Nanoparticle Dispersions. *Nanotechnology* **2007**, *18* (45), No. 455704.